Alternative Al-based Eutectic Systems for Improved Electrical Conductivity

Kentaro Lunn, Benjamin E. MacDonald, Jack Webster, Yanis Cantaloube,
Carl Söderhjelm, Diran Apelian
Advanced Casting Research Center (ACRC)
University of California, Irvine, California, USA

ABSTRACT

Enhancing thermal conductivity in aluminum alloys can drive superior performance and efficiency across diverse engineering applications, including electric vehicle (EV) powertrain components. While most aluminum (Al) alloys produced by high-pressure die casting (HPDC) are based on the aluminum-silicon (Al-Si) hypoeutectic composition range, such as 356, these alloys exhibit suboptimal electrical and thermal conductivity in the as-cast state. Although conductivity can be improved through costly heat treatments, limitations within the Al-Si alloy system persist. Alternative eutectic systems have demonstrated the potential in surpassing both mechanical and conductivity properties of the Al-Si system. However, the relative performance of these novel alternative eutectic systems and the contributions of microstructural features have yet to be established. Therefore, this study bridges this gap by fabricating similar hypoeutectic alloy compositions across various alternative eutectic systems to elucidate the relationship between the eutectic phase structures and electrical conductivity. This research contributes to advancing the understanding of alloy design principles for alternative eutectic systems.

Keywords: alternate eutectic systems, conductivity, high-pressure die casting, aluminum alloys

INTRODUCTION

Thermal management is essential for engineered components and assemblies. Nevertheless, the thermal conductivity of aluminum alloys is often consigned to a lower priority relative to other structural properties despite its importance for thermal management. This oversight can limit performance in circumstances where the thermal conductivity of aluminum is *the* bottleneck in limiting performance. For instance, aluminum engine components require efficient heat dissipation during high-temperature operations to mitigate thermomechanical stresses that could shorten component lifespan.[1] Similarly, heat generated by batteries and electric motors need to be effectively managed through aluminum housing components for optimal performance.[2] Fundamental limitations in electric motor performance arise due to the challenge of dissipating heat from critical components when operating at higher power levels.[3] These situations underscore the necessity to prioritize both conductivity and mechanical properties in aluminum alloys.

High-pressure die casting (HPDC) is the predominant method for producing aluminum automotive components, accounting for over ~60% of the global production of aluminum castings.[2] The HPDC process, like other casting processes, relies upon the advantages of eutectic alloy systems, which were brought to light independently by Rudorff in 1864 and Guthrie in 1875.[4,5] These researchers identified the existence of a minimum of the liquidus curve that Guthrie termed as *eutectic*, referring to the Greek word *eutektos* meaning "easily melted."[4,5]

Eutectic systems solidify at the eutectic point through an invariant reaction, which transpires at a specific temperature and a constant alloy composition.[6] These alloy systems offer a controllable microstructure that can be synthesized in near-equilibrium condition through their invariant reactions and offer superior mechanical properties relative to single phase alloys.[4,6] Furthermore, eutectic systems are preferred for their processability attributed to a combination of good liquidity, low melting temperature, and castability.[4]

The Al-Si systems, featuring Si content between ~4 to 12 wt.%, has been the traditional alloys of choice for casting, accounting for ~80-90% of the global aluminum castings.[7] Its castability is attributed to Si's ability to promote fluidity, mitigate cracking, and minimize shrinkage porosity by improving feedability. Al-Si alloys with less than 12 wt.% Si are classified as hypoeutectic, near 12 wt.% as eutectic, and above 12 wt.% as hypereutectic.[8] The reduced susceptibility to cracking is imparted by a smaller solidification temperature range, which is at Δ78°C (140°F) for 1 wt.% Si and becomes Δ0°C near the eutectic point of 12 wt.% Si.[9]

Silicon has its benefits for processing but significantly compromises the conductivity of Al. As a benchmark, pure Al (99.99% purity) demonstrates outstanding conductivity with electrical conductivity and thermal conductivity of 237 $Wm^{-1}K^{-1}$ and 64.94% IACS (International Annealed Copper Standard), respectively.[7,10,11] Conversely, the thermal conductivity of single crystal Si and polycrystalline Si measured is 145 $Wm^{-1}K^{-1}$ and 15~30 $Wm^{-1}K^{-1}$, respectively, and are both significantly lower than that of pure Al.[1]

This discrepancy in conductivity properties outlines the considerable constraint imposed by utilizing Si as a secondary phase when trying to couple high conductivity with decent mechanical properties. In fact, commercial castable Al-Si alloys are limited to roughly ~50% of both the thermal and electrical conductivity Al (99.99% purity).[9] Table 1 delineates the specific conductivity values for Al-Si alloys in various tempers.

***Table 1. Conductivity Values for Die-C*astable Al-Si Alloys in Various Tempers[7,10]**

Alloy	Temper	Thermal Conductivity $(\frac{W}{m \cdot K})$	Electrical Conductivity (%IACS)
319	As-cast	109	27
360	As-cast	113	30
A360	As-cast	113	28
380	F	96	27
A390	F	134	27
356	T6	151	39~41
A390	T5	134	25

To fully understand the conductivity limitations of Al-Si, there is a need to delve into the fundamental mechanisms that influence the electrical and thermal conductivity of a metallic alloy. Electrical conductivity refers to the ability for electrons to move through a material and is dictated by the unimpeded flow of free electrons through a material.[12] On the other hand, thermal conductivity refers to a material's capacity to transfer heat through a material, a process governed by two primary mechanisms: 1) the propagation of phonons through lattice vibrations and 2) the movement of free electrons.[1] Equation 1[2,7,13] demonstrates that the total thermal conductivity of a metal is the aggregate of its electronic thermal conductivity and phonon thermal conductivity:

$$k_{total} = k_{electron} + k_{phonon} \quad \text{Eqn. 1}$$

The Wiedemann-Franz law proposed relating the electronic contribution to thermal conductivity (k) to electrical conductivity (σ) as noted in Equation 2:[2,7,13]

$$\frac{k_e}{\sigma} = L_0 T \quad \text{Eqn. 2}$$

T is the absolute temperature and L_0 is the Lorentz coefficient, which remains nearly constant for aluminum alloys at an approximate value of $2.1*10^{-8} W\Omega K^{-2}$.[11] This relationship establishes a direct proportionality between a metallic material's thermal and electrical conductivities, however, with notable exceptions such as Si.[2] It's significant to note that the electronic contribution to thermal conductivity is typically between ~10 to 100 times that of phonon contribution.[14]

Therefore, free electron flow is the main determinant of electrical and thermal conductivity for pure metals.[7,12,14] While phonon thermal conductivity is negligible for pure metals, this component becomes significant for metallic alloys due to electron scattering effects.[2] The three primary mechanisms of electron scattering processes include 1) metallic lattice defects 2) electrons deflected via phonons, and 3) interactions amongst electrons.[2,15] Matthiessen's rule states that various contributions to the resistivity of metals due to electron scattering can be summed up to determine the overall electrical resistivity.[2] In theory, this principle can also be applied to study the electronic scattering contributions to thermal resistivity. However, such study is challenging due to the inability to directly measure electronic thermal conductivity and the inherent difficulties in conducting thermal conductivity measurements.[16] Metallurgical features that promote electron scattering and consequently lower thermal conductivity include alloying elements in solid solution, grain boundaries, second-phase inclusions, and porosity.[17] Although pure Al has exceptional thermal and electrical conductivity properties, it lacks sufficient strength for structural applications and cannot be used without strengthening alloying elements.[10] An alloy design conundrum exists because all strengthening methods such as work hardening, solid solution strengthening, and strengthening inevitably lead to a reduction in thermal conductivity.[7,18]

Extensive research has been carried out to discern the microstructural factors influencing the conductivity of Al-Si alloys. It has been established that elevating the Si content from 2 to 12.6 wt.% decreases the electrical conductivity from 47.5 to 30% IACS, a trend attributed to the increased volume fraction of the eutectic Si phase.[19] Previous studies have also established a direct correlation between the eutectic phase dendrite refinement and increased thermal conductivity within the Al-Si system.[1] Another study has pinpointed that higher solidification rates resulted in higher conductivity due to the refinement of both the primary Al and eutectic phase.[19] Porosity is directly associated with reductions in thermal conductivity.[1] Vandersluis' study on a cast Al-Si alloy has assessed that approximately an increase in porosity per 1% can lead to a decrease in thermal conductivity by ~10-20 W/mK.[1,12] Another study attributed both the reduction in porosity and refinement of the eutectic Si phase morphology and size as reasons as to why increased cooling rate during solidification improved conductivity.[7] New Al-Si alloys have been developed to incorporate B to reduce the solid solution content of Zr, V, and Ti, which are particularly detrimental to conductivity.[20]

Significant attention has centered on the morphology of the Si eutectic phase as the critical determinant in the overarching conductivity of Al-Si alloys. In the realm of two-phase eutectic alloys, the mean free path of electrons is determined by alloying elements present in the Al solid

solution but will be further reduced by electron collision with the eutectic phase.[19] This insight is pivotal for understanding that the Sr-induced eutectic morphology modifications improve conductivity through altering the rate of electron collision at the Si eutectic phase.[7,19] While lamellar eutectic Si phase tends to obstruct electrons, its fibrous counterpart is more conducive to electron flow.[7] One proposed hypothesis for this phenomenon is that the rod-like eutectic phase diminishes the projected area of interaction between the eutectic phase and aluminum matrix, increasing the cross-sectional area of the aluminum phase within the eutectic regions that facilitate electron flow.[19] Lumley demonstrated that the aging of Al-Si alloys to modify the eutectic Si into a finer, more spherical structure enhanced thermal conductivity relative to the as-cast state.[2] Mulazimoglu verified that Al-Si-Sr alloys have a lower resistivity by ~5-10% than non-modified Al-Si alloys containing the same level of Si.[19] This improvement was attributed to Sr's ability to refine the eutectic Si phase from a plate-like to a fibrous-like structure, decreasing the resistivity by ~5-10%.[19]

Alternative eutectic systems, including Al-Ni, Al-Fe, Al-Ce, Al-Fe-Ni, and Al-Ca offer promising opportunities for readily processible alloys with superior mechanical and conductivity properties compared to the traditional Al-Si system. The Al-Ca, Al-Ce, and Al-Ni eutectic systems demonstrate a combination of narrow crystallization intervals and workability in annealed state despite a large vol% of intermetallic phases (~10 vol%).[21,22] These specific alternative eutectic systems also demonstrate strength properties on par with Al-Si system alloys without the need of strengthening alloying elements such as Zn, Mg, Cu, Zr, and Sc.[21] The Al-Fe, Al-Ni, and Al-Fe-Ni demonstrate comparable if not better hot tearing susceptibility, fluidity, and mechanical properties with respect to Al-Si with Sr-modifications.[23,24]

Many of these alternative eutectic systems offer superior high temperature stability relative to the Al-Si system as well.[23-26] Limited studies have demonstrated the superior conductivity properties of alternative eutectic systems. Chankitmukong's study demonstrated that hypereutectic Al-Fe and Al-Ni with Zr additions showed superior electrical conductivity to comparable Al-Si system alloys in both the as-cast and aged conditions.[27] Similarly, Medevedev investigated an Al-Ce-La hypoeutectic alloy produced via high pressure torsion, which achieved a combination of decent tensile strength of 500 MPa and high electrical conductivity of 52.2% IACS.[28]

These alternative eutectic systems feature secondary alloying elements with very low solid solubility in Al (Table 2), which presents an intrinsic advantage because alloying elements in solid solution lowers conductivity.[1,2,7,17,18]

Table 2. Solid Solubility of Elements in Al for Alternative Eutectic Systems of Interest[11,29-32]

Element	Invariant Reaction	Temp. C/F	Solid Solubility wt.%	Solid Solubility at. %
Silicon (Si)	Eutectic	580/1076F	1.65	1.59
Nickel (Ni)	Eutectic	640/1184	0.05	0.023
Iron (Fe)	Eutectic	655/1211	0.052	0.025
Cerium (Ce)	Eutectic	638/1180	<0.05	<0.023
Calcium (Ca)	Eutectic	620/1148	<0.1	<0.01

While research has highlighted the potential of alternative eutectic systems, the detailed microstructural factors related to the eutectic phase of each system remain largely uncharted. A comprehensive exploration of this subject necessitates a deep dive into the following facets:

- The electronic & crystal structure of individual elements;
- the inherent conductivity of individual elements;
- the conductivity of relevant intermetallic phases;
- the influence of crystal structure on conductivity; and
- the morphology of the eutectic phase.

In understanding electrical conductivity, it is essential to differentiate between different classes of pure elements based on their respective electron band structures. *Metals* are defined as materials with at least one partially filled electronic band in their ground state, allowing for the flow of current, while *insulators* have all electronic bands either completely empty or full in the ground state, creating an energy gap between the top of the highest filled and the lowest empty bands.[15] This distinction arises from the fact that electrons in a filled electronic band cannot carry current.[15] A special category of *semiconductors* exist that behave as insulators at absolute zero but allow for conduction at higher temperatures below their melting point.[15] The *Fermi level* represents the energy needed to introduce an additional electron into a solid-state material.[15] This level can be conceptualized as a hypothetical energy level where there's a 50% probability of an electron being present under thermodynamic equilibrium.[15] It's vital to understand that in *metals* the Fermi level resides within a delocalized electronic band with states that can conduct current. In contrast, *semiconductors* and *insulators* have Fermi levels far away from states that can carry current.[15]

Clarifying this distinction is critical because Si is a *nonmetallic element* while the secondary alloying elements of the alternative eutectic systems are all *metallic elements*. In the Al-Si system, Si is present as a pure *nonmetal* eutectic phase while the secondary

elements of the alternative eutectic systems are present in the form of *intermetallic phases*, suggesting a fundamental difference in electrical conductivity. Table 3 lists the electronic structure and room temperature stable crystal structure of the key alloying elements of interest.

Table 3. Electronic & Crystal Structure of Key Pure Metals of Interest[9,15]

Element	Electronic Structure	Crystal Structure
Al	[Ne] $3s^2 3p^1$	FCC
Si	[Ne] $3s^2 3p^2$	Diamond cubic
Ni	[Ar] $3d^6 4s^2$	FCC
Fe	[Ar] $3d^8 4s^2$	BCC
Ce	[Xe] $4f^1 5d^1 6s^2$	FCC
Ca	[Ar] $4s^2$	FCC

Understanding both *Fermi surfaces* and *crystal binding* is essential in elucidating the relationship between an element's electronic structure and its electronic conductivity and crystal structure, respectively.

The Fermi surface is a theoretical boundary that separates unfilled electron orbitals from filled electron orbitals at a temperature of absolute zero.[33] A pure metal's electrical properties are fundamentally driven by the volume and shape of its *Fermi surfac*e because changes in electronic state predominantly occur near the boundaries of this surface.[33]

Crystal binding is the attractive electrostatic forces between negative charges of electrons and positive charges of the nuclei that are entirely responsible for the bonding of solids.[33] This binding determines the inherent crystal structure of a pure element. A defining metric is the average number of valence electrons and can be used to relate transitions in crystal structure of alloy systems.[33] For instance, the FCC structure exists between an electron concentration of 1-1.38 while a BCC structure is stable between 1.38-1.48 within the Cu-Zn alloy system.[33] Moreover, theoretical electronic configurations provide insight into why certain crystal structures are implausible. In the case of Al, neither BCC or HCP structures can exist because their theoretical electronic configurations require freer *s*-shell electrons and less *p*-shell covalently bonded electrons relative to the electronic configuration of stable FCC Al.[34]

Aluminum is a trivalent metal with a fermi surface that closely mirrors the free electron surface of an FCC monatomic Bravais lattice with three conduction electrons per atom, a significant contributor to its high conductivity.[15] Moreover, its relatively large number of free electrons about its lattice structure increase its electrical and thermal conductivity.[35]

Si is characterized by covalent bonds with strong directional properties that give rise to its diamond structure.[33] This covalent bond results from Si lacking four electrons with respect to filled shells and results in attractive interactions with overlapping charges.[33] This structure ultimately leads to Si's intrinsic semiconductor characteristics with a band gap of 1.12 eV and its less favorable electrical conductivity compared to metals.[15] However, Si's thermal conductivity is excellent. Studies on the thermal conductivity of pure Si have revealed that lattice vibrations almost entirely account for the thermal conductivity between 300K and 1000K / 27 and 727C (80 and 1340F) and that electronic contributions as indicated by Wiedemann-Franz law are entirely negligible.[36] Accordingly, Si possesses a combination of poor electrical conductivity and excellent thermal conductivity, two seemingly but not necessarily contradicting properties.

Fe, Ni, and Ce are transition metals with the *3d and 4s* electronic band available for conduction.[33] While such characteristics may lead to the assumption that transition metals are highly conductive, the resistivity of the *s* shell electron path is increased due to collisions with the *d* electrons, a significant extra scattering mechanism that is not present for elements with a filled *d* band.[33] This *d* band interaction results in complex Fermi surfaces, corresponding to lower conductivity.[37] These transition metals have crystal binding from inner electron shells and are characterized by high binding energy.[33]

Ca is a divalent metal within the alkaline earth metals that lies in the column of the periodic table immediately to the right of the alkali and noble metals.[15] Alkaline earth metals feature overlapping of the 3s and 3p orbitals that, in turn, facilitate conduction of electrons.[38] Ca's FCC crystal structure may suggest a free-electron like behavior, but the hybridization of the *d* shells results in deviation of the Fermi surface relative to free-electron ones.[39] The Fermi surface of Ca was overall small and disconnected suggesting relatively poor electrical conductivity.[40] The conductivity of divalent metals is considerably less affected with respect to whether the electron *d*-band is filled as in the case for transition metals.[15] The binding energy of bonds formed by conduction electrons are not very strong.[33] Thus, interatomic distances are relatively large in alkaline metals because the kinetic energy of the conduction electrons is lower at larger interatomic distances.[33] This loose binding results in the tendency to form close packed structures such as HCP, FCC, and BCC instead of loose packed structures such as diamond.[33] Complete band calculations indicate that Ca is much less of a free-electron metal and behaves as a semiconductor at extreme pressures around ~14 GPa.[41]

Table 4 lists each key element's thermal conductivity and electrical conductivity measured near room temperature.

Table 4. Thermal and Electrical Conductivity of Pure Elements of Interest at Room Temperature[9]

Element	Thermal Conductivity $(\frac{W}{m \cdot K})$	Electrical Conductivity (%IACS)
Al	~247	~65-66
Si	~156	~0
Ni	70~86	~18.15~22.99
Fe	~78-80.2	~17.59
Ce	~11.3	~2.32
Ca	~126	~49.6

This measured data confirms that alkaline earth metals such as Ca tend to have better conductivities relative to transition metals such as Ni, Fe, and Ce. Si does demonstrate the best thermal conductivity and worst electrical conductivity in its pure form relative to other pure elements, a unique attribute as a semiconductor. Although this data may lead one to believe that the conductivity of pure elements should decide which alternative eutectic system performs the best in terms of thermal and electrical conductivity. However, this is not the case in principle because these elements exist in the form of intermetallic phases with unique crystal structures and morphologies.

An intermetallic is a chemical compound of two or more metals that produce a unique combination of composition, crystal structure, mechanical and chemical properties relative to their respective pure metals.[42] Intermetallic phases form when two or more elements do not follow Hume Rothery rules and/or the solute element exceeds solid solubility.[42] Terada's research has indicated that intermetallic compounds inherently demonstrate greater thermal conductivity than corresponding solid solutions regardless of crystal structures.[43] Terada's previous study on intermetallic compounds demonstrated that they satisfy Wiedemann-Franz law as is the case for pure element and metallic alloys.[44] This, in turn, indicates that electron flow is the dominant carrier for thermal conduction for intermetallic phases.[44]

Intermetallics are bonded by a combination of metallic and ionic bonds that depend upon the differences between the electronegativity of between constituent elements [42]. The intermetallic phase exhibits primarily metallic bonds when the differences between electronegativity are lower and become more ionic as the differences grow. Electronegativity is measured by the Pauling scale and becomes greater depending on the oxidation state of a metal.[45] Table 5 lists the electronegativity of key elements of interest and its difference relative to Al.

Table 5. Electronegativity of Key Elements and Δ with Respect to Al[45]

Element	Electronegativity	Δ vs. Al
Al	1.61	-
Ni	1.91	0.30
Fe	1.83	0.22
Ce	1.12	-0.49
Ca	1.00	-0.61

This criterion alone would suggest that Fe and Ni perform better than other alternative eutectic systems. Each eutectic phase of these alternative alloy systems features unique crystal structures as shown in Table 6.

While research exploring the impact of crystal structure on conductivity is somewhat sparse, certain trends are apparent. In general, more complex crystal structures should increase scattering and lower conductivity.[17] Terada's studies have demonstrated that ordering increases thermal conductivity.[43] For instance, the measured thermal conductivity of an $L1_2$ ordered Ni_3Al structure will exceed that of a theoretical disordered FCC disordered Ni_3Al structure.[43] Furthermore, the thermal conductivity of an intermetallic compound can be characterized as a sum of the contribution of solid solution and effects due to ordering of the crystal structure.[43]

Table 6. Eutectic Phase Crystal Structures[46-51]

Eutectic System	Eutectic Phase
Al-Si	Diamond Si
Al-Ni	Al_3Ni
Al-Fe	$Al_{13}Fe_4$
Al-Ce	$Al_{11}Ce_3$
Al-Fe-Ni	Al_9FeNi
Al-Ca	Al_4Ca

While comprehensive data on every phase is unavailable, there exists a limited pool of information regarding the conductivity properties of the alternative eutectic system phases under consideration.[11] Specifically, the Al_3Ni phase is confirmed to have a thermal conductivity of 30 $Wm^{-1}K^{-1}$, a value that is roughly on par with the upper limit of polycrystalline diamond Si.[1,44] On the other hand, the $Al_{13}Fe_4$ phase is reported to have an exceedingly low thermal conductivity and electrical conductivity of $0.8*10^{-3}$ $Wm^{-1}K^{-1}$ and ~0.000000336 %IACS, respectively.[11]

The eutectic phases of the alternative eutectic systems exhibit distinct morphological differences compared to that of the Al-Si system. The eutectic phase of the Al-Ce system exhibits a platelet-like morphology whereas that of the Al-Ca has a very thin lamellar structure.[31,32] On the other hand, Al-Fe, Al-Ni, and Al-Fe-Ni all feature eutectic phases with a rod-like structure.[23,24] It is worth noting that significantly improved conductivity properties

are observed through modifying the eutectic Si phase to a rod-like morphology.[7,19]

Inherent limitations of the Al-Si alloy system warrant the investigation of novel alternative eutectic alloys for an augmented combination of thermal conductivity and mechanical properties. Currently, our comprehension of how these distinct eutectic phases impact conductivity remains limited. There is potential value in exploring how the fundamental structure and conductivity properties of eutectic phases vary across the alternative eutectic systems. This work aims to elucidate the significance of the eutectic phase and eutectic phase morphology in determining an alloy's electrical conductivity. Such insight may facilitate the design and optimization of novel alloys within these alternative eutectic systems.

EXPERIMENTAL PROCEDURE

Six experimental hypoeutectic alloys were cast by melting a mixture of pure Al (99.9% purity) with Al-50Si wt.%, Al-10Fe wt.%, Al-36Ni wt.%, Al-8Ce wt.%, and Al-10Ca wt.% master alloys using two *Thermolyne* box furnaces. The compositions of these alloys and corresponding eutectic phases are listed in Table 7.

Table 7. Target Compositions & Eutectic Phases of Alternative Eutectic Systems of Interest

Eutectic System	Target Composition (wt.%)
Al-Si	Al-7Si
Al-Ni	Al-3Ni
Al-Fe	Al-0.9Fe
Al-Ce	Al-6Ce
Al-Fe-Ni	Al-0.8Fe-0.9Ni
Al-Ca	Al-3.75Ca

These compositions were selected through *PANDAT CALPHAD* simulations that intended to control the fraction of primary solidified Al to comparable to microstructures achieved in previous studies and listed in Table 8.

Table 8. Target Primary (A) Phase Fraction Amongst Alternative Eutectic Systems

Eutectic System	Primary (α) Phase (%)
Al-Si	51
Al-Fe	52
Al-Ni	50
Al-Fe-Ni	46
Al-Ce	38
Al-Ca	50

An argon gas shielding apparatus was used within the furnace to feed argon into the crucible specifically containing the Al-Ca melt to minimize oxidation. Upon placing a crucible with the desired master alloys of interest, the furnace was raised to 750C (1382F), held at temperature for 1 h, and then the crucible was removed from the furnace for manual mixing. After this step, the crucibles returned to the furnace, held at 750C (1382F) for an additional hour, and stirred one last time prior to casting. This process was carried out at 850C (1562F) for Al-Fe and Al-Fe-Ni melts due to issues regarding master alloys settling at the bottom of the crucibles. Subsequently, the crucibles were removed from the furnace and molten metal was immediately poured into a copper mold and Arc Spark Optical emission spectroscopy (OES) mold that were preheated to 125 and 350 ± 10°C (257 and 662 ± 18°F), respectively, to ensure consistent cooling rates during the casting process. An infrared thermometer was used to verify the temperature of the molds before and during the casting process.

A 3 ± 0.1 mm sample was sectioned at a consistent location near the center of the casting for each alternative eutectic alloy sample cast in Cu molds. Each sample was metallographically prepared to a 320-grit finish for x-ray diffraction (XRD) characterization with a *Rigaku Ultima III* x-ray diffractometer. Subsequently, the sample was mounted and metallographically prepared to a surface finish of 0.06 μm for further optical microscopy using an *Olympus GX53* microscope and field emission electron microscopy coupled with energy dispersive spectroscopy (EDS) using an *FEI Quanta 3D FEG* electron microscope.

Image analysis was performed on both optical and scanning electron micrographs using *ImageJ* software. This analysis was used to determine several key parameters including defects, the secondary dendrite arm spacing (SDAS), primary Al dendrite arm length (PDAL), phase area fractions, and eutectic phase thickness.

Various methods exist for measuring the Secondary Dendrite Arm Spacing (SDAS) of aluminum alloys. Vandersluis' study examined 5 different approaches for accomplishing SDAS measurements.[52] The significance of this comparison lies in the fact that the direct measurement of the SDAS (*method E*) yields an average SDAS comparable to that obtained through an indirect method (*method D*). This finding indicates that a more convenient method, namely *method D*, can be utilized without sacrificing measurement quality. Consequently, *method D* was chosen for use in this study for SDAS measurements.

The primary Al dendrite arm length (PDAL) obtained through measuring the length of randomly selected dendrites. This measurement aimed to investigate whether a correlation existed between this feature and the conductivity performance of an alternative eutectic system.

Trainable Weka Segmentation (TWS), a machine learning based approach for pixel classification, was implemented to obtain area fractions of the primary aluminum phase and eutectic region. This method was applied to 4-6 micrographs at identical magnifications for each alloy sample.

Manual line measurements of eutectic phases were taken from SEM micrographs at magnifications ranging from 5000x to 10000x to determine the eutectic phase thickness.

Arc Spark Optical emission spectroscopy (OES) was performed using an *Ametek Spectrolab S* unit to verify the composition of the cast samples. This measurement process involves ablating a sample of material in a controlled environment saturated with argon gas using an arc spark. The spectrometer then analyzes the spectrum of light emitted by the ablated material and cross-references it with an established commercial database to verify the composition.

However, it's worth noting that the Al-Ca sample has a Ca content that exceeded existing commercial databases and could not be accurately measured through this method. In such a case, compositions were verified through EDS elemental maps data. Measured and validated compositions were fed into *PANDAT* simulations to predict present phases and verify phase stabilities.

The electrical conductivity measurements were conducted using an *Olympus Nortec 600* eddy current detection device, which operates by applying an alternating current and measuring the resulting voltage to determine electrical conductivity in terms of International Annealed Copper Standard (%IACS). Given that Eddy current testing is sensitive to the sample geometry, all measurements were taken from the same location on the samples cast for the OES measurements. For each sample, five measurements were taken, and prior to each analysis, a calibration procedure was performed to minimize sensor drift.

RESULTS

The electrical conductivity of the various hypoeutectic samples is shown in Figure 1 in the order of least to greatest electrical conductivity.

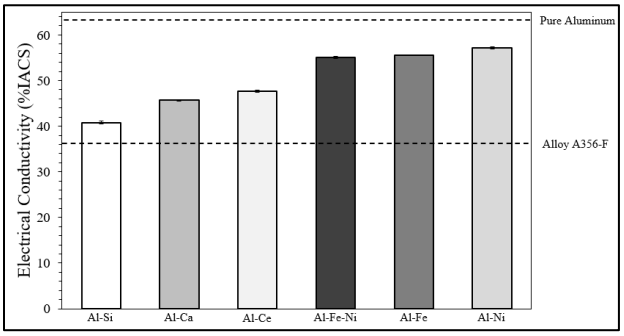

Figure 1. Electrical conductivity measurements of hypoeutectic samples using the identical casting process with pure Al and alloy A356-F literature values for Reference 9.

The tabulated data associated with the Figure 1 is shown in Table 9.

Table 9. Electrical Conductivity Measurement Data

Alloy	Electrical Conductivity (%IACS)
Hypoeutectic Al-Si	40.81 ± 0.34
Hypoeutectic Al-Ca	45.70 ± 0.15
Hypoeutectic Al-Ce	47.66 ± 0.18
Hypoeutectic Al-Fe-Ni	55.07 ± 0.17
Hypoeutectic Al-Fe	55.62 ± 0.06
Hypoeutectic Al-Ni	57.09 ± 0.24

All the alternative eutectic systems exhibit superior conductivity properties compared to the Al-Si system. Although conductivity of these alloys is less than pure Al, they are all inherently more conductive than alloy A356 in the as-cast condition.[9] The ranking in conductivity of these hypoeutectic alternative eutectic systems is the following in the order of best to worst: Al-Ni, Al-Fe, Al-Fe-Ni, Al-Ce, and Al-Ca. Microstructural analysis will be conducted to understand *why* the conductivity ranking is in this order. Thus, comprehensive microstructural analysis was conducted to delineate correlations between microstructural parameters and the overall conductivity ranking of these alternative eutectic systems.

Before approaching microstructural details, it is important to understand how close the targeted composition and consequent predicted primary (α) phase is present. Table 10 provides a comparison of targeted and measured composition across all samples.

Table 10. Targeted vs. Measured Composition Across Hypoeutectic Samples

Eutectic System	Target Composition(wt.%)	Measured Composition (wt. %)
Al-Si	Al-7Si	Al-6.81Si ± 0.03
Al-Ni	Al-3Ni	Al-3Ni ± 0.02
Al-Fe	Al-0.9Fe	Al-1.03Fe ± 0.01
Al-Ce	Al-6Ce	Al-6.14Ce ± 0.09
Al-Fe-Ni	Al-0.8Fe-0.9Ni	Al-0.91Fe-0.92Ni ± 0.01
Al-Ca	Al-3.75Ca	Al-3.64Ca

This composition was fed into an additional PANDAT simulation to compare the original predicted vs. a revised prediction of primary (α) phase fraction (Table 11).

Table 11. Original vs. Revised Prediction Primary (α) Phase Fraction Amongst Alternative Eutectic Systems

Eutectic System	**Targeted Prediction Primary (α) Phase (%)**	**Revised Prediction Primary (α) Phase (%)**
Al-Si	51	53
Al-Fe	52	45
Al-Ni	50	49
Al-Fe-Ni	46	39
Al-Ce	38	36
Al-Ca	50	51

This prediction provides evidence that the quantity of eutectic phase is not necessarily the definitive predictor of conductivity as observed by the poor performance of the Al-Si and Al-Ca samples with the most amount of primary Al and consequent least amount of eutectic phase. Given this initial comparison, the first and foremost significant feature to characterize across all eutectic systems is the eutectic phase. Figure 2 is an example of an optical micrograph taken at an identical magnification for each alternative eutectic system for comparison.

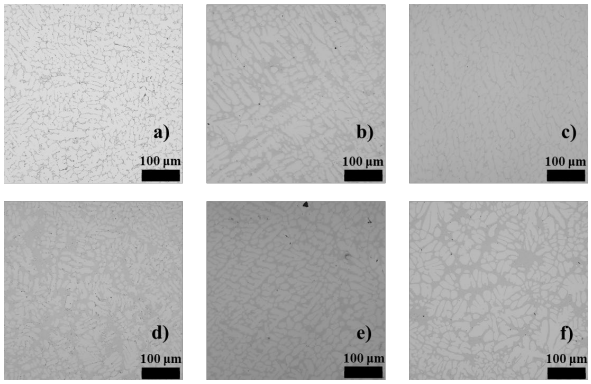

Figure 2. Optical micrographs of hypoeutectic (a) Al-Si (b) Al-Ni (c) Al-Fe (d) Al-Ce (e) Al-Fe-Ni (f) Al-Ca alloy.

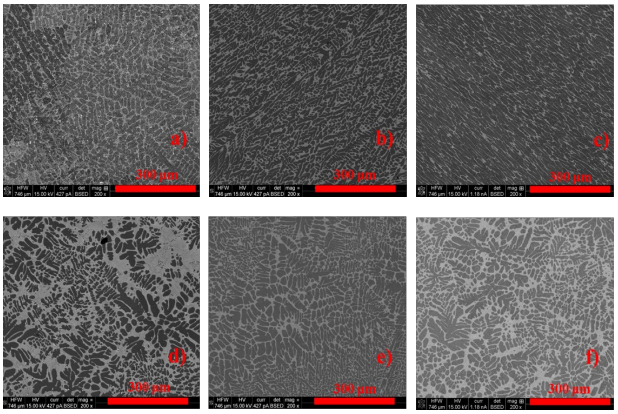

Figure 3. SEM Micrograph of hypoeutectic (a) Al-Si (b) Al-Ni (c) Al-Fe (d) Al-Ce (e) Al-Fe-Ni, and (f) Al-Ca alloy at 1000x magnification.

To gain a comprehensive understanding of how the microstructure affects conductivity, it's essential to quantify these eutectic phases and regions. It's worth noting that all samples exhibited dendritic microstructures except for the Al-Fe alloy sample, which therefore could not be assessed for SDAS and PDAL (Primary Al Dendrite Arm Length). Additional micrographs were captured near the center of each sample and were used to determine the SDAS and PDAL values, as presented in Table 12.

Table 12. SDAS and PDAL of Alternative Eutectic System Samples

Eutectic System	SDAS (µm)	PDAL (µm)
Al-Si	12.40 ± 2.59	224.32 ± 42.95
Al-Fe	-	-
Al-Ni	9.07 ± 1.43	84.32 ± 13.04
Al-Fe-Ni	10.32 ± 2.67	103.53 ± 32.50
Al-Ce	9.71 ± 2.08	114.88 ± 34.82
Al-Ca	11.63 ± 2.10	70.04 ± 15.58

The SDAS measurements suggest a loose relationship between higher conductivity with smaller SDAS or vice versa. The SDAS may vary to some extent but appear nearly identical amongst Al-Ni, Al-Fe-Ni, and Al-Ce, which are amongst the better performers. Al-Si and Al-Ca are the worst and 2nd worst in terms of electrical conductivity and are correlated with the largest and 2nd largest SDAS. Vandersluis' study has noted that the refinement of SDAS due to cooling rate changes was a relatively negligible factor influencing thermal conductivity for Al-Si systems.[1,13]

It is not readily apparent if there is a correlation between PDAL and conductivity. The Al-Si alloy, which performs the worst, has the longest PDAL, while the second-worst performer has the shortest PDAL. The PDAL values for

the remaining samples are similar. In principle, a greater PDAL would imply a higher mean free path of electrons, facilitating electron conduction through primary Al dendrite pathways. However, overall trends may suggest the length of the primary dendrite arms in the microstructure are relatively negligible factors in determining an alternative eutectic system's conductivity. This observation may suggest that the PDAL and contiguity of the primary Al matrix may not necessarily be directly related.

Backscattered electron micrographs were acquired to calculate the area fraction of the eutectic region in comparison to the primary aluminum phase. Z-contrast was used to visually highlight the distinct phases based on their atomic number differences. An example for each alternative eutectic system is shown in Figure 3.

Several additional micrographs were taken of each alternative eutectic system at a lower magnification for area fraction measurements. The results of these measurements are shown in Table 13.

Table 13. Area Fraction of Phases Derived from SEM Micrographs

Eutectic System	Primary (α) Area%
Al-Si	65.79 ± 2.96
Al-Fe	76.54 ± 2.06
Al-Ni	77.92 ± 1.55
Al-Fe-Ni	76.24 ± 2.00
Al-Ce	61.24 ± 2.00
Al-Ca	75.23 ± 2.96

The eutectic system samples analyzed using PANDAT are anticipated to exhibit primary Al phase fractions in the descending order of: Al-Fe, Al-Si, Al-Ni, Al-Ca, Al-Fe-Ni, and Al-Ce. The measured area fractions indicated the following order: Al-Ni, Al-Fe, Al-Fe-Ni, Al-Ca, Al-Si, and Al-Ce. Although there is a degree of variability, the trends are relatively consistent except for Al-Si and Al-Fe-Ni. Al-Fe, Al-Ni, and Al-Fe-Ni are all high performers in terms of conductivity and exhibit the lowest eutectic region area fractions. Conversely, Al-Ca which shares a similar eutectic region area fraction, exhibits notably inferior electrical conductivity. This observation implies other microstructural structure features of the Al_4Ca eutectic phase have a greater influence beyond merely the amount present. A similar argument applies to the $Al_{11}Ce_3$ eutectic phase considering that the Al-Ce sample has by far the highest eutectic phase region area fraction but surpasses both the Al-Ca and Al-Si alloy in terms of electrical conductivity. These findings underscore the pivotal role of the eutectic phase itself over mere quantity in determining the overall alloy's conductivity performance.

The thickness of each eutectic phase was measured using high magnification SEM micrographs to further characterize the morphology of the eutectic phase and understand its relationship to conductivity. Since the Al-Ca exhibited both globular and lamellar eutectic phase microstructures, measurements representative of each region were taken as well. An example of each eutectic phase is shown in Figure 4.

The thickness measurements taken of each eutectic phase is shown in Table 14.

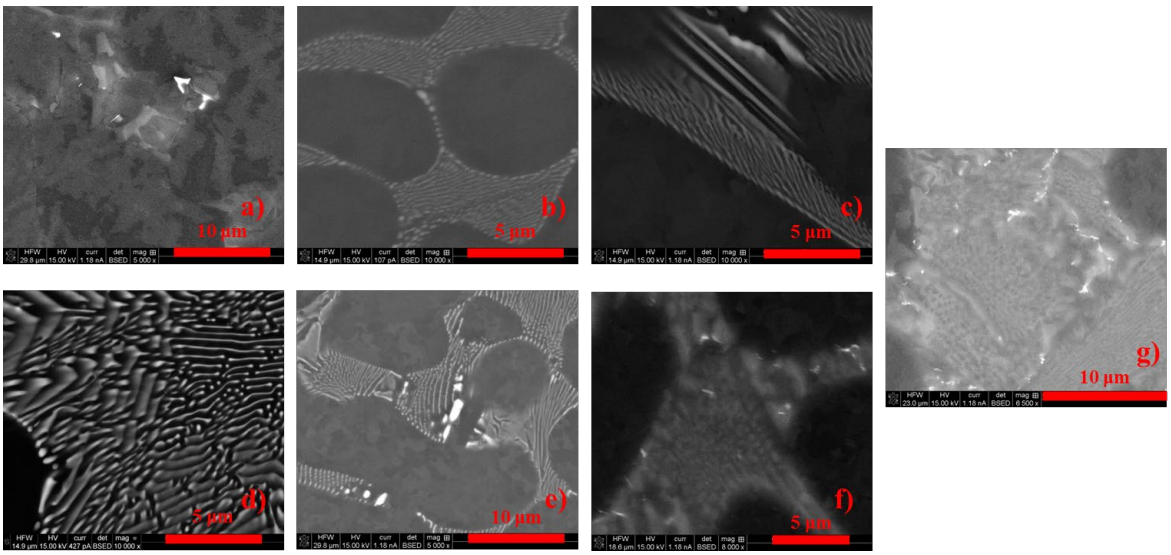

Figure 3. SEM micrograph of hypoeutectic (a) Al-Si (b) Al-Ni (c) Al-Fe (d) Al-Ce (e) Al-Fe-Ni, and (f) Al-Ca (globular) (g) Al-Ca (lamellar) eutectic phase at high magnifications.

Table 14. Eutectic Phase Thickness

Alloy	Eutectic Phase Thickness (nm)
Al-Si	522.80 ± 90.72
Al-Fe	105.2 ± 14.63
Al-Ni	97.00 ± 9.30
Al-Fe-Ni	111.00 ± 10.33
Al-Ce	201.30 ± 63.77
Al-Ca (Globular Region)	250.8 ± 44.45
Al-Ca (Lamellar Region)	172.00 ± 32.38

A strong, direct relationship exists between the eutectic phase thickness and electrical conductivity such that thinner phases consistently demonstrate superior conductivity. For reference, nearly identical eutectic phase thickness measurements have been taken in Fan's prior research on the Al_3Ni phase, which indicated that the diameter of the rod-like structure was approximately 100 nm.[53] The eutectic phase of Al-Fe, Al-Ni, and Al-Fe-Ni are all rod-like by nature and are top performers in terms of conductivity.

The next best performer Al-Ce features a platelet-like eutectic phase while the worst performers Al-Ca and Al-Si both exhibit a lamellar eutectic phase. It is worth noting that other studies on the Al-Ca denote the thin structure of the Al_4Ca eutectic phase, which agrees with this study.[32] Although the Al_3Fe and Al_3Ni phase have starkly different conductivities, both the Al-Fe and Al-Ni hypoeutectic samples exhibit similar high conductivity.[11,44] This suggests that the physical structure of the eutectic phase may be a main determinant of conductivity.

There are other confounding variables that may be influencing the conductivity of each alternative eutectic alloy such as defects, impurity elements, alloying elements in solid solution, and impurity phases. These parameters will be examined individually to verify whether these defects may play a role.

The entire surface of each hypoeutectic sample was optically examined, and defects observed on this surface were classified into two categories: porosity or inclusions, determined by their visual characteristics. Examples of such identified defects are shown in Figure 5.

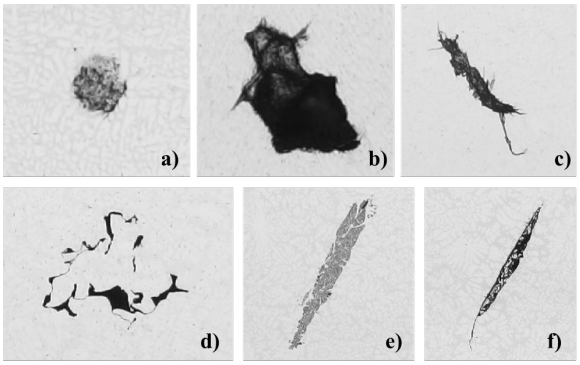

Figure 4. Examples of (a, b, c) porosity and (d, e, f) oxide inclusions identified within the surface.

It is worth noting that porosity examples a-b and c were obtained from the Al-Ni and Al-Ce samples, respectively. Oxide inclusion examples d and e-f were taken from the Al-Ce and Al-Ca samples, respectively. The quantity of such defects was quantified across the entire sample surface and are listed in Table 15.

Table 15. Area Fractions of Identified Defects for Each Alternative Eutectic System

Eutectic System	Relative Density %	Inclusion Area %
Al-Si	99.93%	0.027%
Al-Fe	99.98%	0.065%
Al-Ni	99.96%	0.007%
Al-Fe-Ni	99.98%	0.011%
Al-Ce	99.97%	0.024%
Al-Ca	100%	0.100%

The number of visible defects remained quite low in all the eutectic systems. Notably, the Al-Ca alloy showed a slightly higher incidence of defects compared to the other samples, which could possibly be linked to calcium's tendency to oxidize.

However, this data implies that variations in conductivity among the alternative eutectic systems are unlikely to be substantially influenced by disparities in defect quantity.

Optical Emission Spectroscopy (OES) measurements were used to determine the exact composition of each cast sample. Alloying element content other than the eutectic phase elements can be considered as impurities with respect to alloy design and have a detrimental impact on conductivity and are listed in Table 16.

Table 16. Key Impurity Elements Detected by OES (wt. %)

Eutectic System	Si Impurity (wt. %)	Fe Impurity (wt. %)	Ni Impurity (wt. %)	Mn Impurity (wt. %)	Ti Impurity (wt. %)	Cr Impurity (wt. %)	V Impurity (wt. %)
Al-Si	-	0.0508	0.0022	0.0009	0.0008	0.0007	<0.0003
Al-Fe	0.0150	-	0.0019	0.0048	<0.0003	0.0006	<0.0003
Al-Ni	0.0135	0.0287	-	0.0008	0.0003	0.0001	0.0004
Al-Fe-Ni	0.0158	-	-	0.0045	0.0003	0.0006	<0.0003
Al-Ce	0.0453	0.0910	0.0305	0.0011	0.0055	0.0034	0.0085

Table 17. Nominal Impurity Content (wt. %)

Alloy	Impurity Content
Al-Si	0.09
Al-Fe	0.07
Al-Ni	0.10
Al-Fe-Ni	0.07
Al-Ce	0.36

This data reveals that the impurity levels in Al-Si, Al-Fe, Al-Ni, and Al-Fe-Ni are quite similar, suggesting that differences in conductivity may not necessarily be confounded by impurity content. On the other hand, Al-Ce exhibits a significantly higher impurity content relative to the other alternative eutectic systems, which could impact its conductivity. It's important to highlight that the Al-Ce alloy demonstrated superior conductivity relative to the Al-Si alloy despite having significantly higher impurity content. Elements that are alloyed within a solid solution tend to have a more adverse impact on conductivity when compared to elements that are not in solution. Some elements, such as Cr, V, Ti, Mn, and Fe are especially detrimental when present in solid solution.[2,17,20] These elements cause an increase in resistivity (measured in μΩ-cm) of 4.00, 3.58, 2.88, 2.94, and 2.56 per 1 wt.% addition, respectively.[54] The content of these key impurity elements along with common impurity elements identified by OES are shown in Table 17.

These impurity elements are in general very low except for the Al-Ce alloy. Common impurity elements of Si, Fe, Ni, and Mn were examined. Fe was identified as a substantial impurity across Al-Si, Al-Ni, and Al-Ce. However, it is difficult to argue that impurity content is driving the differences in conductivity across alternative eutectic systems since they are comparable across all alloy systems. Comparison of impurity content, if anything, reinforces the inherent superior conductivity characteristics associated with alternative eutectic systems that can provide superior conductivity despite having higher impurity element content.

SEM-EDS was used to determine the quantity of the key secondary eutectic-forming alloying element detected in the aluminum solid solution and are listed in Table 18.

The precision of EDS points analysis is fundamentally limited due to the interaction of the electron beam with surrounding regions.

Table 18. Alloying Element Content in Al Solid Solution (wt.%)

Alloy	Si	Fe	Ni	Ce	Ca
Al-Si	1.84 ± 0.53				
Al-Fe		0.13 ± 0.04			
Al-Ni			0.11 ± 0.17		
Al-Fe-Ni		0.14 ± 0.07	0.10 ± 0.04		
Al-Ce				0.06 ± 0.07	
Al-Ca					0.18 ± 0.18

A likely scenario is that the EDS spectra is identifying alloying elements in adjacent eutectic phases and the amount of the key eutectic phase alloying element is significantly lower than measured. The worst conductivity associated with Al-Si could be tied with its highest solid solution eutectic phase alloying element content.

Otherwise, the pattern regarding the relationship between alloying content in solid solution vs. conductivity are not very pronounced amongst the alternative eutectic systems. For instance, Al-Fe-Ni contains nearly double the alloying element content relative to Al-Fe and Al-Ni, yet its conductivity is only slightly worse. Furthermore, Al-Ce has the least amount of alloying element content in solid solution, but it does not perform the best in terms of conductivity. This data suggests that the level of alloying element content in the aluminum solid solution is not as crucial a factor as other microstructural parameters when it comes to explaining the differences in conductivity among various eutectic systems.

The confirmed compositions obtained through a combination of Optical Emission Spectroscopy (OES) and Scanning Electron Microscopy with Energy Dispersive X-ray Spectroscopy (SEM/EDS) were employed in *PANDAT* simulations to predict secondary phases shown in Table 19.

Table 19. Predicted Secondary Phases from PANDAT Simulations

Alloy	Predicted Secondary Phases
Al-Si	Si, AlFeSi
Al-Fe	$Al_{13}Fe_4$, AlFeSi
Al-Ni	Al_3Ni, Al_9FeNi
Al-Fe-Ni	Al_9FeNi, $Al_{13}M_4$
Al-Ce	$Al_{11}Ce_3$, AlCeSi, $AlCeSi_2$, $Al_{10}RM_2$, $Al_{13}M_4$, AlFeSi, Al_9FeNi
Al-Ca	Al_4Ca, $Al_{13}M_4$, AlFeSi, Ca_3Si_4

The phases detected via x-ray diffraction are listed in Table 20.

Table 20. Measured Secondary Phases from X-ray Diffraction

Alloy	Detected Secondary Phases
Al-Si	Si
Al-Fe	$Al_{13}Fe_4$
Al-Ni	Al_3Ni
Al-Fe-Ni	Al_9FeNi
Al-Ce	$Al_{11}Ce_3$, AlCeSi, $AlCeSi_2$
Al-Ca	Al_4Ca, Ca_3Si_4

CONCLUSIONS

This comprehensive study has provided valuable insights into the intricate relationship between microstructural parameters and electrical conductivity across various alternative eutectic alloy systems. Key findings from this study include the following:

- The electrical conductivity measurements unequivocally demonstrated that all alternative eutectic systems outperformed the Al-Si system.
- Conductivity ranking (best to worst): Al-Ni, Al-Fe, Al-Fe-Ni, Al-Ce, Al-Ca, and Al-Si.
- These trends hold for thermal conductivity.
- There was a direct, strong correlation between thinner eutectic phases and superior conductivity.
- The best performing alloy systems all exhibited a rod-like eutectic phase followed up by platelet-like and then lamellar morphology.
- Secondary Dendrite Arm Spacing (SDAS) exhibited a loose correlation in which finer spacing was related to higher conductivity.
- Primary Al Dendrite Arm Length (PDAL) did not reveal any discernible patterns influencing conductivity.
- Confounding variables such as defects, impurity elements, and alloying elements appear to be relatively negligible variables compared to the eutectic phase microstructure.

These insights hold promise in guiding future alloy design endeavors within novel alternative eutectic systems that promise superior conductivity and mechanical properties.

ACKNOWLEDGMENTS

The authors express their gratitude to the member companies of the Advanced Casting Research Center (ACRC) for their continued guidance and support.

REFERENCES

1. P. Emadi, B. Andilab and C. Ravindran, "Engineering lightweight aluminum and magnesium alloys for a sustainable future," *Journal of the Indian Institute of Science*, vol. 102, no. 1, pp. 405-420 (2022).
2. R.N. Lumley, "Thermal Conductivity of Aluminum High-Pressure Die Castings," in Fundamentals of Aluminum Metallurgy: Recent Advances, Cambridge, Woodhead Publishing, pp. 217-246 (2018).
3. K. Bennion, "Electric Motor Thermal Management Research Annual Progress Report," National Renewable Energy Laboratory, Golden (2017).
4. B. Chanda, G. Potnis, P.P. Jana and J. Das, "A review on nano-/ultrafine advanced eutectic alloys," *Journal of Alloys and Compounds*, vol. 827, pp. 1-49 (2020).
5. F. Guthrie, "LII. On eutexia," *The London, Edinburgh, and Dublin Philosophical Magazine and Journal of Science*, vol. 17, no. 108, pp. 462-482 (1884).
6. W. Smith and J. Hashemi, “Foundations of Materials Science and Engineering,” New York: McGraw-Hill Education, pp. 351-354 (2019).
7. A. Zhang and Y. Li, "Thermal Conductivity of Aluminum Alloys - A Review," Materials, vol. 16, no. 2972, pp. 1-21 (2023).

8. J.R. Davis, “ASM Specialty Handbook: Aluminum and Aluminum Alloys,” Materials Park: ASM International, pp. 92-94 (1993).
9. ASM International, “ASM Handbook Volume 2: Properties and Selection: Nonferrous Alloys and Special-Purpose Materials,” Materials Park: ASM International, pp. 178, 239, 569-643, 2922-3144 (2004).
10. G.E. Totten and D.S. MacKenzie, “Handbook of Aluminum Vol. 1: Physical Metallurgy and Processes,” Boca Raton: CRC Press, pp. 51, 881-882, 910, 928 (2003).
11. L. F. Mondolfo, Aluminum Alloys: Structure and Properties, Boston: Butterworth & Co, 1979, pp. 96, 282-289, 338-342.
12. E. Vandersluis and C. Ravindran, "The Role of Porosity in Reducing the Thermal Conductivity of B319 Al Alloy with Decreasing Solidification Rate," *JOM: the Journal of the Minerals, Metals & Materials Society*, vol. 71, no. 6, pp. 2072-2077 (2019).
13. E. Vandersluis, P. Emadi, B. Andilab and C. Ravindran, "The Role of Silicon Morphology in the Electrical Conductivity and Mechanical Properties of As-Cast B319 Aluminum Alloy," *Metallurgical and Materials Transactions A* , vol. 51, no. 4, pp. 1874-1886 (2020).
14. M. Ohring, “Engineering Materials Science,” San Diego: Academic Press, pp. 559-605 (1995).
15. N.W. Ashcroft and N.D. Mermin, “Solid State Physics,” Fort Worth: Saunders College Publishing, pp. 284-311,322-326, 374-393 (1976).
16. T. Farrell and D. Greig, "The thermal conductivity of nickel and its alloys," *Journal of Physics C: Solid State Physics,* vol. 2, no. 8, pp. 1465-1473 (1969).
17. M. Makhlouf, L. Wang, D. Apelian and L. Yang, "Thermal Conductivity of Aluminum Diecasting Alloys," *AFS Transactions*, vol. 107, pp. 501-505 (1999).
18. J. Miyake, G. Ghosh and M.E. Fine, "Design of High-Strength, High-Conductivity Alloys," *MRS Bulletin*, vol. 21, no. 6, pp. 13-18 (1996).
19. M.H. Mulazimoglu, R.A. Drew and J.E. Gruzleski, "The Electrical Conductivity of Cast Al-Si Alloys in the Range 2 to 12.6 wt% Si," *Metallurgical Transactions A*, vol. 20, no. 3, pp. 383-389 (1989).
20. A. Pithan and H. Koch, "Modifications of Aluminum Alloys for High Thermal Stress," *International Journal of Metalcasting*, vol. 9, no. 1, pp. 67-71 (2015).
21. S.O. Rogachev, E.A. Naumova, E A. Lukina, A.V. Zavodov and V.M. Khatkevich, "High Strength Al-La, Al-Ce, and Al-Ni Eutectic Aluminum Alloys Obtained by High-Pressure Torsion," *Materials*, vol. 14, pp. 1-18 (2021).
22. N.A. Belov, K.A. Batyshev and V.V. Doroshenko, "Microstructure and phase composition of the eutectic Al-Ca alloy, additionally alloyed with small additives of zirconium, scandium and manganese," *Non-ferrous Metals*, vol. 43, no. 2, pp. 49-54 (2017).
23. T. Koutsoukis and M. Makhlouf, "An alternative eutectic system for casting aluminum alloys I. Casting ability and tensile properties," *Light Metals*, pp. 277-281 (2015).
24. T. Koutsoukis and M. Makhlouf, "Alternatives to the Al-Si Eutectic System in Aluminum Casting Alloys," *International Journal of Metalcasting,* vol. 10, no. 3, pp. 342-247 (2016).
25. Z. Bian, Y. Xiao, J. Geng, L. Hu, Z. Chen, M. Wang, D. Chen and H. Wang, "Optimizing Zr addition method to improve the comprehensive high temperature performance of Al-Fe-Ni-Sc eutectic alloy," *Journal of Alloys and Compounds*, vol. 866, pp. 1-8 (2021).
26. Z.C. Sims, O.R. Rios, D. Weiss, P.A. Turchi, A. Perron, J.R. Lee., L.T. Tian, J.A. Hammons, M. Bagge-Hansen, T.M. Willey, K. An, Y. Chen, A.H. King and S.K. McCall, "High Performance Aluminum-Cerium Alloys for High-Temperature Applications," *Advanced Casting Technologies*, pp. 1-12 (2018).
27. S. Chankitmunkong, D.G. Eskin and C. Limmaneevichitr, "Effects of Ultrasonic Melt Processing on Microstructure, Mechanical Properties, and Electrical Conductivity of Hypereutectic Al-Si, Al-Fe, and Al-Ni with Zr Additions," *Light Metals 2021*, The Minerals, Metals & Materials Series, pp. 192-197 (2021).
28. A.E. Medvedev, M.Y. Murashkin, N.A. Enikeev, I. Bikmukhametov, R.Z. Valiev, P.D. Hodgson and R. Lapovok, "Effect of the eutectic Al-(Ce,La) phase morphology on microstructure, mechanical properties, electrical conductivity and heat resistance of Al-4.5(Ce,La) alloy after SPD and subsequent annealing," *Journal of Alloys and Compounds*, vol. 796, pp. 321-330 (2019).
29. H.B. Henderson, J.A. Hammons, A.A. Baker, S.K. McCall, T.T. Li, A. Perron, Z.C. Sims, R.T. Ott, F. Meng, M.J. Thompson, D. Weiss and O. Rios, "Enhanced thermal coarsening resistance in a nanostructured aluminum-cerium alloy produced by additive manufacturing," *Materials & Design*, vol. 209, pp. 1-12 (2021).
30. C. Zhang, P. Peng, H. Lu, H. Gao, Y. Wang, J. Wang and B. Sun, "Orientation relationships and interface structure between Al11Ce3 and Al in Al-Ce

eutectic," *Journal of Materials Research and Technology*, vol. 18, pp. 693-704 (2022).
31. Y. Liu, R.A. Michi and D.C. Dunand, "Cast near-eutectic Al-12.5 wt.% Ce alloy with high coarsening and creep resistance," *Materials Science & Engineering: A*, vol. 767, pp. 1-9 (2019).
32. S.O. Rogachev, E.A. Naumova, E.S. Vasileva, M.Y. Magurina, R.V. Sundeev and A.A. Veligzhanin, "Structure and mechanical properties of Al-Ca alloys processed by severe plastic deformation," *Materials Science & Engineering A*, vol. 767, no. 138410, pp. 1-7 (2019).
33. C. Kittel and P. McEuen, "Introduction to Solid State Physics," Hoboken: John Wiley & Sons, Inc., pp. 221-252 (2004).
34. Y. Xie and X. Liu, "Electronic structures and physical properties of pure aluminum metal," *Science in China Series E: Technologies Series*, vol. 42, no. 6, pp. 603-608 (1999).
35. H.S. Abdo, A.H. Seikh, J.A. Mohammed and M.S. Soliman, "Alloying elements effects on electrical conductivity and mechanical properties of newly fabricated Al based alloys produced by conventional casting process," *Materials*, vol. 14, no. 14, pp. 1-10 (2021).
36. H.R. Shanks, P.D. Maycock, P.H. Sidles and G.C. Danielson, "Thermal conductivity of silicon from 300 to 1400°K," *Physical Review*, vol. 130, no. 5, pp. 1743-1748 (1963).
37. J. Schäfer, M. Hoinkis, E. Rotenberg, P. Blaha and R. Claessen, "Fermi surface and electron correlation effects of ferromagnetic iron," *Physical Review B*, vol. 72, no. 15, pp. 1-11 (2005).
38. B.K. Tanner, "Introduction to the physics of electrons in solids," Cambridge: Cambridge University Press, p. 95 (2003).
39. P. Blaha, C and J. Callaway, "Electronic structure and Fermi surface of calcium," *Physical Review B*, vol. 32, no. 12, pp. 7664-7669 (1985).
40. S.L. Altmann, A.R. Harford and R.G. Blake, "The band structure and Fermi surface of calcium," *Journal of Physics F: Metal Physics*, vol. 1, no. 6, pp. 791-805 (1971).
41. S.L. Altmann and A.P. Cracknell, "The Fermi surface and conductivity of calcium," *Proceedings of the Physical Society*, vol. 84, no. 5, pp. 761-765 (1964).
42. A.R. Paul, M. Mukherjee and D. Singh, "A Critical Review on the Properties of Intermetallic Compounds and Their Application in the Modern Manufacturing," *Crystal Research and Technology*, vol. 57, no. 3, pp. 1-19 (2021).
43. Y. Terada, K. Ohkubo, T. Mohri and T. Suzuki, "A comparative study of thermal conductivity in alloys and compounds," *Materials Science and Engineering A*, vol. 278, pp. 292-294 (2000).
44. Y. Terada, K. Ohkubo, T. Mohri and T. Suzuki, "Thermal Conductivity of Intermetallic Compounds with Metallic Bonding," *Materials Transactions,* vol. 43, no. 12, pp. 3167-3176 (2002).
45. J. Emsley, "The Elements," 3rd Edition, Oxford: Oxford University Press (1998).
46. The Materials Project, "Materials Data on Si by Materials Project," United States (2020).
47. The Materials Project, "Materials Data on Al_3Ni by Materials Project," United States (2020).
48. The Materials Project, "Data retrieved from the Materials Project for $Al_{13}Fe_4$ (mp-1202900) from database version v2022.10.28," https://next-gen.materialsproject.org/materials/mp-1202900 (Link last accessed 04-04-2024.)
49. The Materials Project, "Data retrieved from the Materials Project for Ce_3Al_{11} (mp-1213865) from database version v2022.10.28." https://materialsproject.org/materials/mp-1213865 (Link last accessed 04-04-2024.)
50. The Materials Project, "Materials Data on Al_9Co_2 by Materials Project," United States (2020).
51. The Materials Project, "Materials Data on $CaAl_4$ by Materials Project," United States (2020).
52. E. Vandersluis and C. Ravindran, "Comparison of Measurement Methods for Secondary Dendrite arm Spacing," *Metallography, Microstructure, and Analysis,* vol. 6, no. 1, pp. 89-94 (2017).
53. Y. Fan and M.M. Makhlouf, "The Al-Al_3Ni Eutectic Reaction: Crystallography and Mechanism of Formation," *Metallurgical and Materials Transactions A*, vol. 46A, pp. 3808-3812 (2015).
54. W.A. Dean and K.R. Van Horn, "Chapter 6 Effects of Alloying Elements and Impurities on Properties," in Aluminum Vol. I. Properties, Physical Metallurgy and Phase Diagrams, Metals Park, American Society for Metals, pp. 174-176 (1967).